

Square Wave Voltammetry for Two-Step Surface Reductions

John J. O'Dea and Janet G. Osteryoung*

Department of Chemistry, North Carolina State University, Raleigh, North Carolina 27695-8204

Strongly adsorbed species on an electrode surface are used to create a stable, redox-modified surface. Square wave voltammetry is then used to degrade the surface electrochemically, as evidenced by the resulting voltammetric response. This process can be mathematically modeled as a quasi-reversible surface reaction coupled with a first-order irreversible surface reaction of the product. This is the simplest possible model that can explain a two-step surface reduction. Exemplary calculations for square wave voltammetry show a wide variety of peak shapes depending on rate constants and square wave amplitude. The reduction of Dimethyl Yellow (4-(dimethylamino)azobenzene) adsorbed on mercury is accurately described by this model. Characteristic parameters of the overall surface process are obtained from voltammograms by using the two-step model with nonlinear least-squares analysis (COOL). For Dimethyl Yellow in Britton–Robinson buffer (pH 6.00) at a surface concentration of 17.3 pmol cm⁻², these parameters are as follows: standard potential, $E_1^0 = -0.397 \pm 0.001$ V vs SCE; transfer coefficient for the first step, $\alpha_1 = 0.43 \pm 0.02$; rate constant for the first step, $k_1^0 = 103 \pm 8$ s⁻¹; transfer coefficient for the second step, $\alpha_2 = 0.11 \pm 0.04$; and rate constant for the second step, k_2^0 (referenced to E_1^0) = 11.1 ± 1.7 s⁻¹. Uncertainties are 95% confidence intervals derived from a pool of 11 voltammograms collected at different square wave amplitudes ($E_{sw} = 0$ –100 mV).

In previous work, we have treated charge transfer reactions of adsorbates using as examples the totally irreversible reduction of midazolam¹ and the quasi-reversible reduction of azobenzene.² Many adsorbed species, however, do not undergo a single simple surface reaction. The cathodic reduction of an organic adsorbate usually activates an intermediate that reacts either cathodically again or with the surrounding environment. Such secondary reactions are easily detected using square wave voltammetry,³ which repetitively drives the potential of the electrode to values selected to cause oxidization and reduction. Chemical complexity of a surface process may be revealed or concealed by the shape of the voltammetric response.

In this work, we examine the effect of a second, irreversible reaction on the normal redox cycling of a surface. Such reactions are observed or expected under sufficiently harsh conditions for a wide variety of systems, including redox-modified surfaces, conducting polymer films, sensors, and “self-assembled” microstructures populated with redox sites. Modeling the surface reactions as first-order processes provides a basis for quantitative interpretation of square wave voltammograms. With a suitable model, the COOL algorithm⁴ also permits the refinement of electrochemical parameters from experimental data. The resulting rate constants characterize the complex behavior of the system. Here we develop a mathematical description of a two-step surface reaction and demonstrate its application to the redox behavior of an adsorbed dye. We restrict ourselves to the first-order model, which is widely applicable to pseudo-first-order reduction of organic compounds in buffered aqueous solution.

Electrochemical data concerning the surface electron transfer reactions of azo dyes are sparse, in spite of the widespread use of such reactions in textiles and newly found applications in nonlinear optics^{5,6} and optoelectronics.^{7,8} Electrochemical kinetics and energetics yield information about molecular energy levels and may be useful for predicting the photochemical reactivity⁹ of these types of materials. Here we demonstrate the application of a two-step model using the surface reduction of the azo dye Dimethyl Yellow (4-(dimethylamino)azobenzene) as an example. Adsorptive accumulation combined with square wave voltammetry has already been used for the trace level determination of azobenzene.¹⁰ In this case, the reversible turnover of the azo/hydrazo moiety is exploited for increased analytical sensitivity. Dimethyl Yellow also undergoes such redox cycling on the electrode surface. This cycling constitutes the first step of a two-step reduction model. In mildly acid solutions, the hydrazo derivative produced by the first step gradually degrades to amines by reductive cleavage of the nitrogen–nitrogen bond. Cleavage to amines destroys the hydrazo group and any possibility for

(1) O'Dea, J. J.; Ribes, A.; Osteryoung, J. G. *J. Electroanal. Chem.* **1993**, *345*, 287.

(2) O'Dea, J. J.; Osteryoung, J. G. *Anal. Chem.* **1993**, *65*, 3090.

(3) Osteryoung, J. G.; O'Dea, J. J. Square Wave Voltammetry. In *Electroanalytical Chemistry*, Vol. 14; Bard, A. J., Ed.; Marcel Dekker: New York, 1986; pp 209–308.

(4) O'Dea, J. J.; Osteryoung, J. G.; Lane, T. *J. Phys. Chem.* **1986**, *90*, 2761.

(5) Ross, D. L.; Blanc, J. Photochromism by *cis-trans* Isomerization. In *Techniques in Chemistry*, Vol. 3, Photochromism; Brown, G. H., Ed.; Wiley-Interscience: New York, 1975; pp 471–556.

(6) Rau, H. Azo Compounds. In *Photochromism. Molecules and Systems*; Durr, H., Bouas-Laurent, H., Eds.; Elsevier: New York, 1990; pp 165–192.

(7) Yabe, A.; Kawbata, Y.; Niino, H.; et al. *Thin Solid Films* **1988**, *160*, 33.

(8) Yariv, E.; Reisfeld, R.; Weiss, A. *Proceedings of the SPIE*, Optoelectronics and Applications in Industry and Medicine, Vol. 1972, 8th Meeting on Optical Engineering in Israel, 1992; pp 46–54.

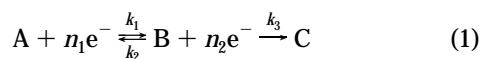
(9) Rifi, M. R.; Covitz, F. H. *Introduction to Organic Electrochemistry*; Marcel Dekker: New York, 1974; p 7.

(10) Xu, G.; O'Dea, J. J.; Mahoney, L. A.; Osteryoung, J. G. *Anal. Chem.* **1994**, *66*, 808.

further redox cycling. The irreversible degradation of surface electroactivity serves as the second step of the two-step model.

MATHEMATICAL MODEL

Consider the surface reaction in which A interconverts with B while B is concurrently and irreversibly reduced to C. Both steps are first-order.



Here, n_1 is the number of electrons transferred in the first step, and n_2 is the number of electrons transferred in the second step. The total surface concentration of adsorbates, Γ^* , is defined as the sum of concentrations of reactants and products.

$$\Gamma^* = \Gamma_A + \Gamma_B + \Gamma_C \quad (2)$$

The corresponding dimensionless surface concentrations of A, B, and C are defined by

$$A = \Gamma_A / \Gamma^* \quad (3)$$

$$B = \Gamma_B / \Gamma^* \quad (4)$$

$$C = \Gamma_C / \Gamma^* \quad (5)$$

The rate equations for the two steps are

$$dA/dt = k_2 B - k_1 A \quad (6)$$

$$dB/dt = k_1 A - k_2 B - k_3 B \quad (7)$$

$$dC/dt = k_3 B \quad (8)$$

Laplace transformation of rate eqs 6 and 7 gives

$$s\bar{A} - A^0 = k_2 \bar{B} - k_1 \bar{A} \quad (9)$$

$$s\bar{B} - B^0 = k_1 \bar{A} - k_2 \bar{B} - k_3 \bar{B} \quad (10)$$

where s is the Laplace transform variable and A^0 and B^0 are the dimensionless surface concentrations of A and B, respectively, at $t = 0$. \bar{A} and \bar{B} are the transformed variables. This system of two equations is solved for \bar{A} and \bar{B} to give the time domain solutions for A and B:

$$A = \frac{[A^0(\gamma_1 - \kappa_2 - \kappa_3) - B^0 \kappa_2] e^{-\gamma_1} - [A^0(\gamma_2 - \kappa_2 - \kappa_3) - B^0 \kappa_2] e^{-\gamma_2}}{(\gamma_1 - \gamma_2)} \quad (11)$$

and

$$B = \frac{[B^0 \gamma_1 - \kappa_1(A^0 + B^0)] e^{-\gamma_1} - [B^0 \gamma_2 - \kappa_1(A^0 + B^0)] e^{-\gamma_2}}{(\gamma_1 - \gamma_2)} \quad (12)$$

Dimensionless rate constants κ_1 , κ_2 , and κ_3 are defined such that

$$\kappa_1 = \kappa_1 / t \quad (13)$$

$$\kappa_2 = \kappa_2 / t \quad (14)$$

$$\kappa_3 = \kappa_3 / t \quad (15)$$

and γ_1 and γ_2 are defined such that

$$g_1 = \gamma_1 / t \quad (16)$$

$$g_2 = \gamma_2 / t \quad (17)$$

and g_1 and g_2 are further specified by

$$g_1 = \frac{(k_1 + k_2 + k_3) - \sqrt{(k_1 + k_2 + k_3)^2 - 4k_1 k_3}}{2} \quad (18)$$

$$g_2 = \frac{(k_1 + k_2 + k_3) + \sqrt{(k_1 + k_2 + k_3)^2 - 4k_1 k_3}}{2} \quad (19)$$

The current corresponding to the conversion of A to B remains to be found. Applying the definitions for κ_1 and κ_2 to the rate equation for A (eq 6) gives

$$dA/dt = \frac{(\kappa_2 B - \kappa_1 A)}{t} \quad (20)$$

The current due to the first step of the process is

$$i_1 = -n_1 F A_e \Gamma^* dA/dt \quad (21)$$

where i_1 is the current in amperes, A_e is electrode area (cm^2), and F is the Faraday constant (96 484.6 C/equiv). Substitution of the right hand side of eq 20 for dA/dt gives

$$i_1 = -n_1 F A_e \Gamma^* \frac{(\kappa_2 B - \kappa_1 A)}{t} \quad (22)$$

The dimensionless current for the first reaction step, Ψ_1 , is defined such that

$$i_1 = \frac{n_1 F A_e \Gamma^*}{t} \Psi_1 \quad (23)$$

Eliminating i_1 and combining eqs 22 and 23 gives

$$\Psi_1 = \kappa_1 A - \kappa_2 B \quad (24)$$

Applying the definition of κ_3 to the rate equation for C (eq 8) gives

$$dC/dt = \frac{\kappa_3 B}{t} \quad (25)$$

The current due to the second step of the process is

$$i_2 = n_2 F A_e \Gamma^* dC/dt \quad (26)$$

where i_2 is the current in amperes. Substitution of the right hand side of eq 25 for dC/dt gives

$$i_2 = n_2 F A_e \Gamma^* \frac{\kappa_3}{t} B \quad (27)$$

The dimensionless current for the second reaction step, Ψ_2 , is defined by

$$i_2 = \frac{n_2 F A_e \Gamma^*}{t} \Psi_2 \quad (28)$$

Eliminating i_2 and combining eqs 27 and 28 gives

$$\Psi_2 = \kappa_3 B \quad (29)$$

The dimensionless current for the overall two-step process, Ψ , is defined by

$$i = i_1 + i_2 = \frac{(n_1 + n_2) F A_e \Gamma^*}{t} \Psi \quad (30)$$

where $(n_1 + n_2)$ is the total number of electrons transferred, and i is the current for the overall process. The quantity Ψ is a linear combination of Ψ_1 and Ψ_2 weighted to reflect the stoichiometry (eq 1):

$$\Psi = \frac{n_1 \Psi_1 + n_2 \Psi_2}{(n_1 + n_2)} \quad (31)$$

In Butler–Volmer formalism, the potential-dependent rate constants, k_1 , k_2 , and k_3 , are given by

$$k_1 = k_1^0 e^{-\alpha_1(n_1 F/RT)(E-E_1^0)} \quad (32)$$

$$k_2 = k_1^0 e^{(1-\alpha_1)(n_1 F/RT)(E-E_1^0)} \quad (33)$$

$$k_3 = k_2^0 e^{-\alpha_2(n_2 F/RT)(E-E_2^0)} \quad (34)$$

where R is the gas constant, T is the absolute temperature, E_1^0 is the standard potential of the A–B couple, and E_2^0 is an arbitrarily chosen reference potential for the B–C couple. We choose E_2^0 to be equal to E_1^0 . This allows the rate constant for the second reaction step to be independent of the experimental choice of reference electrode. The parameter E is the potential of the electrode specified by the waveform, α_1 is the charge transfer coefficient for the A–B couple, α_2 is the charge transfer coefficient for the B–C couple, k_1^0 is the standard rate constant for charge transfer for the A–B couple, and k_2^0 is the standard rate constant for charge transfer for the B–C couple referenced to E_1^0 .

The dimensionless standard rate constants are defined by

$$\kappa_1^0 = k_1^0 t \quad (35)$$

$$\kappa_2^0 = k_2^0 t \quad (36)$$

With the substitution of E_1^0 for E_2^0 , the potential-dependent dimensionless rate constants are

$$\kappa_1 = \kappa_1^0 e^{-\alpha_1(n_1 F/RT)(E-E_1^0)} \quad (37)$$

$$\kappa_2 = \kappa_1^0 e^{(1-\alpha_1)(n_1 F/RT)(E-E_1^0)} \quad (38)$$

$$\kappa_3 = \kappa_2^0 e^{-\alpha_2(n_2 F/RT)(E-E_1^0)} \quad (39)$$

Equations 11 and 12 show that the dimensionless concentrations A and B are the sum of two exponentials controlled by macroscopic rate constants, γ_1 and γ_2 . This form is classically described as “ill conditioned”, and extraction of two rate constants from a single transient in the time domain may be difficult. However, in square wave voltammetry, many transients are produced at widely different reaction rates as a consequence of the pulse sequence of the applied potential. These transients are sampled and used to construct a square wave voltammogram. The model is then reconciled with this ensemble of current measurements via nonlinear least squares.

Currents for multipulse waveforms such as the waveform for square wave voltammetry are calculated by recursion. During each pulse, A and B react at rates fixed by the potential-dependent rate constants for that pulse. These rate constants are found from eqs 37–39. The current at the end of the step is given by Ψ in eq 31. The concentrations of A and B remaining on the electrode at the end of the pulse are given by eqs 11 and 12. Residual A and B continue to react at rates fixed by the potential-dependent rate constants of the next pulse. The current at the end of the next pulse is again given by Ψ . Dimensionless currents over the entire course of the waveform are thus computed recursively. The ensemble of currents plotted against the base staircase potential constitutes the voltammogram. Because each current is computed from an expression in closed form, the computation of complete voltammograms is very fast.

The shape of any particular voltammogram is a function of 10 parameters: n_1 , n_2 , T , ΔE_s (square wave step height), E_{sw} (square wave amplitude), α_1 , α_2 , κ_1^0 , κ_2^0 , and E_1^0 . Five of these 10 parameters are either known or experimentally controlled. The remaining five parameters, α_1 , α_2 , κ_1^0 , κ_2^0 , and E_1^0 , are generally unknown and sought. Calculation of working curves applicable for all combinations of these parameters is not required for analysis and is neither a practical nor a useful exercise. Relatively few calculated voltammograms are sufficient to show trends in peak shape(s) as the lifetime of the intermediate decreases. Examples of separated, split, overlapped, and coincident net peaks will be considered.

The appearance of complex voltammograms is better understood by visualizing the partial currents due to each step of the reduction. These contributions are proportional to Ψ_1 and Ψ_2 from eqs 24 and 29, respectively. In physical reality, of course, these partial currents are inseparable, and only the combined dimensionless current, Ψ , calculated from eq 31, is directly comparable with experiment.

For exemplary calculations, both reductions are cast as two-electron transfers with $\alpha_1 = \alpha_2 = 0.5$. Unless otherwise noted, the value $\kappa_1^0 = 0.1$ is used for the quasi-reversible step. The model waveform is characterized by a step height of 5 mV and an amplitude 25 mV at 25 °C, typical of experimental applications. The remaining degree of freedom, κ_2^0 , is varied over several orders of magnitude to produce a variety of peak shapes. Dimensionless currents $\Psi_1/2$, $\Psi_2/2$, and Ψ are plotted against the base staircase of the waveform using the standard potential of the A–B couple

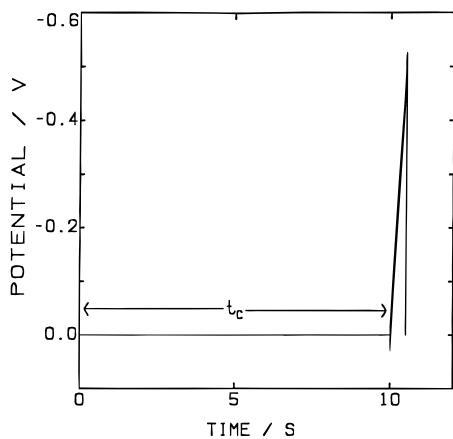


Figure 1. Potential program for adsorptive stripping with preconcentration and square wave detection.

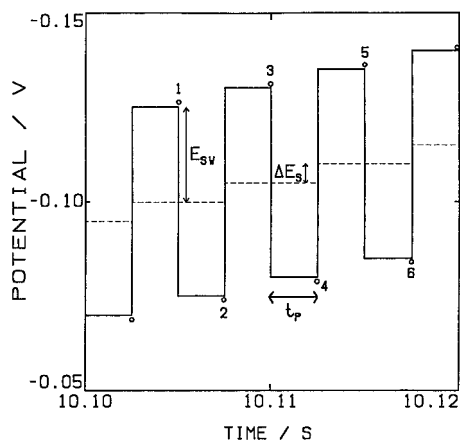


Figure 2. Square wave waveform nomenclature. E_{sw} is the square wave amplitude measured one-half peak-to-peak, ΔE_s the square wave step height, and t_p is the characteristic pulse time of the waveform.

as the reference. The factors of one-half arise because each reduction contributes only half of the total number of electrons passed. The combined current Ψ (Figures 3C, 4C, and 5C) is then easily seen as the arithmetic sum of components $\Psi_1/2$ and $\Psi_2/2$.

Figure 3 shows calculated voltammograms for $\kappa_2^0 = 1 \times 10^{-5}$. The peaks are well separated. Here, the intermediate is long lived and is available at the surface for redox cycling until it is destroyed by much more negative potentials. The two processes are effectively isolated. Considered by itself, Figure 3A shows the simple quasi-reversible reduction of A. Likewise, Figure 3B shows the simple irreversible reduction of a surface populated by only the intermediate. Each of these cases has been treated previously in the literature.^{1,2}

If the quasi-reversible step is somewhat faster, for example $\kappa_1^0 = 2$, the first peak splits, because the forward and reverse currents are skewed. This shift in relative peak position occurs because, for large values of κ_1^0 , $\kappa_2 B$ and $\kappa_1 A$ are not both large in the same potential range (eq 22). In other words, if the reaction is very fast, the reactants are completely consumed before the current is measured. This combination of parameters produces a total of three peaks in the net current for the two processes, as shown in Figure 4.

Figure 5 shows calculated voltammograms for $\kappa_2^0 = 1 \times 10^{-3}$. The net peaks are somewhat overlapped. In this case, a significant fraction of the intermediate is destroyed as it is cycled by the

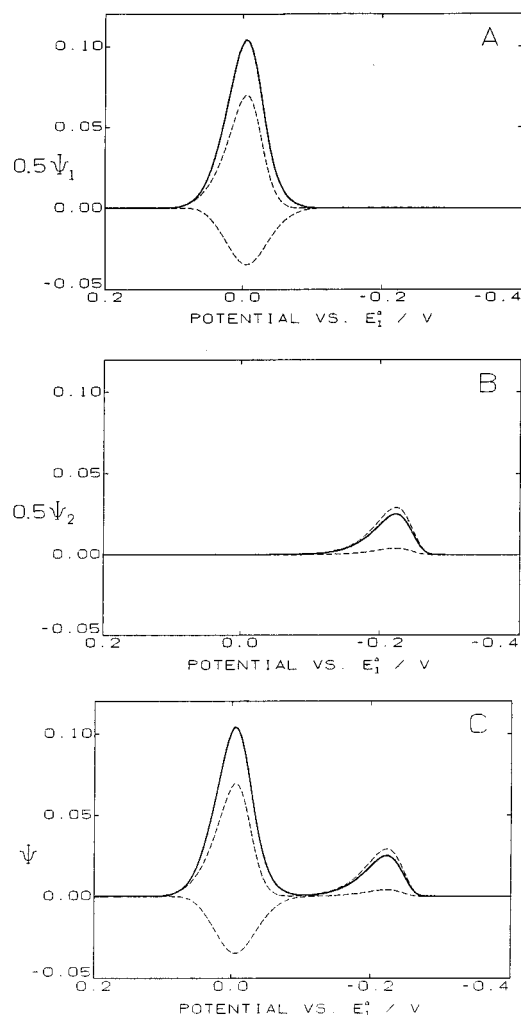


Figure 3. Calculated voltammograms for $\kappa_1^0 = 0.1$, $\kappa_2^0 = 1 \times 10^{-5}$. Forward currents are the upper dashed curves. Reverse currents are the lower dashed curves. Net currents are solid curves. (A) $0.5 \Psi_1$, dimensionless current due the quasi-reversible step. (B) $0.5 \Psi_2$, dimensionless current due the irreversible step. (C) Ψ , dimensionless current for the total process.

alternating potentials of the waveform. The currents due to the individual reaction steps are also slightly distorted. Figure 5A is not identical to Figure 3A, and Figure 5B is not a mere translation of Figure 3B. Uniquely shaped contributions from each reaction are a result of competition for the intermediate. The effect of the followup reaction is more exaggerated for $\kappa_2^0 = 1$, as shown in Figure 6. These conditions correspond to a short-lived intermediate on the surface. A single net current peak is found for an overall four-electron reaction. Current contributions from the first and second reductions are grossly distorted from their isolated quasi-reversible and irreversible forms.

EXPERIMENTAL SECTION

Materials. All reagents used were reagent grade unless otherwise noted. Britton–Robinson buffer (pH 6.00) was prepared by mixing equal amounts of 0.1 M boric and 0.1 M phosphoric acids, titrating to the desired pH with 2 M NaOH, and diluting to volume with Millipore Milli-Q water. Dimethyl Yellow (4-(dimethylamino)azobenzene, Fluka) was used as received.

Instrumentation. An EG&G PARC Model 283 potentiostat, remotely controlled by a personal computer (Gateway 2000 4DX2-50V 486), was used for all voltammetric measurements.

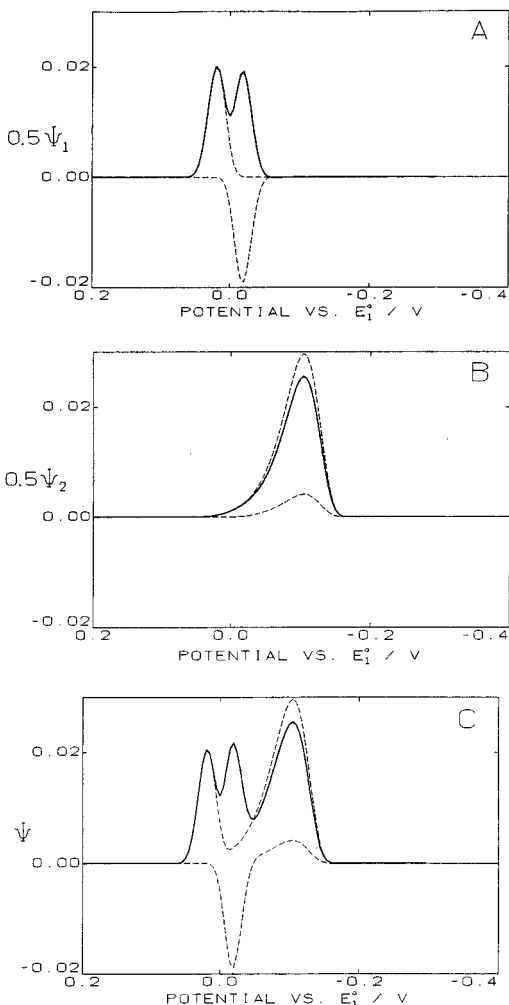


Figure 4. Calculated voltammograms for $\kappa_1^0 = 2$, $\kappa_2^0 = 1 \times 10^{-3}$. Forward currents are the upper dashed curves. Reverse currents are the lower dashed curves. Net currents are solid curves. (A) $0.5 \Psi_1$, dimensionless current due the quasi-reversible step. (B) $0.5 \Psi_2$, dimensionless current due the irreversible step. (C) Ψ , dimensionless current for the total process.

The software employed for experimental control is functionally equivalent to the EG&G PARC 270 software. Solution pH was measured with a Corning Model 220 pH meter using a general purpose combination electrode calibrated against Metreapak pH-dryon buffer standards.

Cell and Electrodes. A Bioanalytical Systems Inc. controlled growth mercury electrode (CGME), Model EF-1400, equipped with a $150 \mu\text{m}$ i.d. beveled capillary, was used for the working electrode. Triple-distilled mercury (Bethlehem Apparatus Co.) was used in the CGME. Dislodge and dispense functions were controlled with external TTL levels supplied by a Quatech S12000 data acquisition system. A drop dispense time of 350 ms was used. This produced an electrode area of 0.03306 cm^2 , as determined by drop weight. An EG&G PARC Model K0077 saturated calomel electrode was used as the reference electrode. A platinum wire served as the counter electrode. All solutions were deaerated using vanadous chloride and amalgamated zinc according to Meites.¹¹ The sample cell was water jacketed and thermoregulated at $25.0 \pm 0.1 \text{ }^\circ\text{C}$. The cell was further sealed from the outside

(11) Meites, L. *Polarographic Techniques*, 2nd ed.; John Wiley & Sons: New York, 1965; p 89.

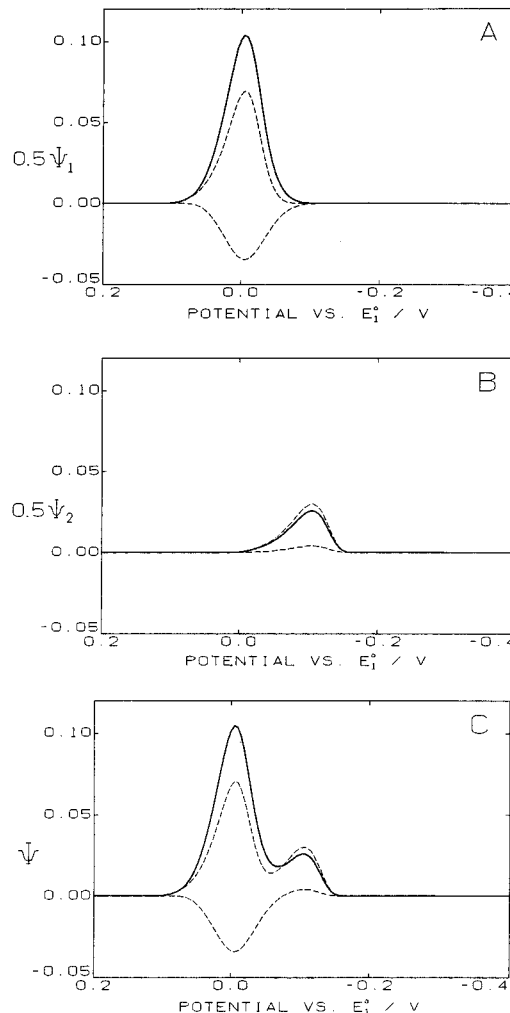


Figure 5. Calculated voltammograms for $\kappa_1^0 = 0.1$, $\kappa_2^0 = 1 \times 10^{-3}$. Forward currents are the upper dashed curves. Reverse currents are the lower dashed curves. Net currents are solid curves. (A) $0.5 \Psi_1$, dimensionless current due the quasi-reversible step. (B) $0.5 \Psi_2$, dimensionless current due the irreversible step. (C) Ψ , dimensionless current for the total process.

atmosphere by a plastic bushing placed around the capillary at the capillary access hole.

Procedures. Adsorptive stripping square wave voltammetry consists of accumulation and detection steps, as shown in Figures 1 and 2. The first step is accumulation of the analyte at the electrode surface. The electrode is held at a conditioning potential, E_c , for a period of conditioning time, t_c . The conditioning potential is chosen such that the analyte accumulates on the electrode surface by adsorption without reaction. For Dimethyl Yellow, a conditioning potential of -0.20 V vs SCE was used during accumulation. Conditioning times were generally limited to a few seconds in order to minimize the influence of adventitious surfactants on electrode kinetics. The solution near the electrode surface is depleted of reactant during the conditioning time, so that the diffusion current during the relatively short stripping step is negligible.

The detection step shown in Figure 2 consists of scanning the potential from an initial value, E_i , to a final value, E_f , with square wave modulation. The waveform is a square wave of frequency $f = 1/(2t_p)$ and amplitude E_{sw} superimposed on a staircase of step height ΔE_s . The quantity t_p is the characteristic pulse width of the waveform. Currents are sampled at the end of each pulse, as

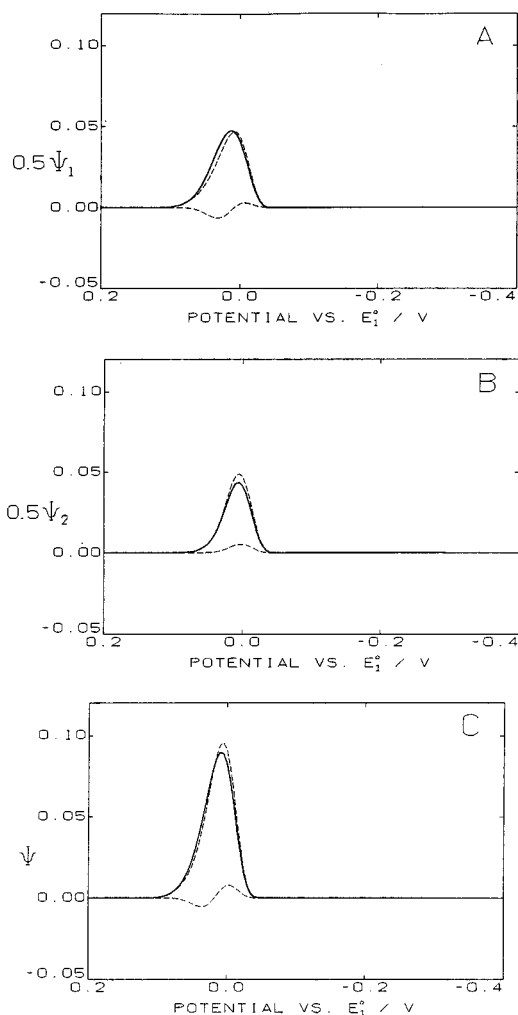


Figure 6. Calculated voltammograms for $\kappa_1^0 = 0.1$, $\kappa_2^0 = 1$. Forward currents are the upper dashed curves. Reverse currents are the lower dashed curves. Net currents are solid curves. (A) $0.5 \Psi_1$, dimensionless current due the quasi-reversible step. (B) $0.5 \Psi_2$, dimensionless current due the irreversible step. (C) Ψ , dimensionless current for the total process.

indicated by the small, numbered circles. The net current voltammogram is obtained by subtracting the even-numbered reverse current from the corresponding odd-numbered forward current and plotting the difference versus the base staircase potential. In this work, E_i is coincident with E_c ; that is, the stripping sequence begins from the conditioning potential. Background currents were negligible and were not subtracted.

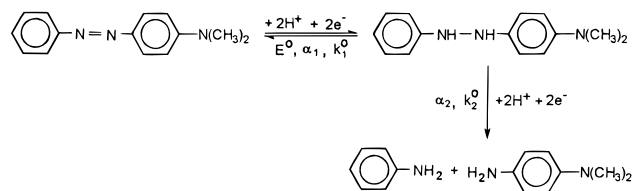
RESULTS AND DISCUSSION

Dimethyl Yellow^{12,13} is an acid–base indicator ($pK_a = 3.3$) existing in two distinct forms depending on pH, namely, the red protonated quinoid and the yellow neutral azoid. At pH 6, the neutral yellow form predominates. Simple experiments varying the conditioning potential, E_c , over the range 0.0 to -0.34 V vs SCE show that the dye is uniformly well adsorbed without potential dependence. At more negative potentials, Dimethyl Yellow reduces directly at the electrode surface, and concentration of the dye before detection is not possible.

Changing the square wave amplitude produces a variety of forward, reverse, and net peak shapes, as shown in Figure 7. For $E_{sw} = 0$ mV (Figure 7A), the square wave waveform degenerates into a simple staircase and approximates an ordinary linear scan at 500 mV/s. Currents sampled at the end of the staircase tread (reverse currents) are shown as the lower dashed curve. The sensitivity of the staircase waveform is relatively poor. The net square wave peak current obtained for $E_{sw} = 30$ mV (Figure 7B) is more than 8 times greater than the staircase peak current for the same step height and frequency. The full width of the peak at half-height is also reduced from 64 to 51 mV. In this case, the advantage of square wave voltammetry for detection of surface reactions is clearly realized in terms of increased sensitivity and resolution.

Increasing the square wave amplitude to 60 mV (Figure 7C) causes a 33 mV positive shift in peak potential and the appearance of a second peak at -0.43 V in the net current. As is evident from the inspection of the forward and reverse currents, most of the amplitude of the second peak is due to the anodic reaction. Increasing the square wave amplitude to 100 mV (Figure 7D) effectively extinguishes the reverse current contribution. The process appears to be completely irreversible, although the net peak current decreases by only 19% compared with the values of Figure 7C.

The changes in voltammetric response shown in Figure 7 cannot be explained by a simple quasi-reversible process as observed with the parent compound, azobenzene.² This elaborate behavior suggests that more than one reaction is involved and that a combination of processes needs to be modeled. A two-step model for reduction of adsorbed Dimethyl Yellow is shown below.



The first step is a two-electron, quasi-reversible reduction yielding the hydrazo derivative. On the voltammetric time scale, the azo/hydrazo moiety can “turn over” many times, following a pulse waveform through both reducing and oxidizing potentials. A strong differential (net) square wave signal is developed under these circumstances, as can be seen in Figure 7B. Indeed, ultratrace quantities of the parent compound, azobenzene, have been detected by using this method.¹⁰

The hydrazo form is subject to competition between oxidation and irreversible reductive cleavage, as shown in the second step of the model. For the parent compound, azobenzene, the two reduction steps are well separated in potential. In Dimethyl Yellow, the dimethylamino substituent increases the basicity of the azo group and facilitates protonation and cleavage of the nitrogen double bond. The reduction potential of the hydrazo form shifts to more positive values and overlaps the quasi-reversible response of the first step. Cleavage to amines destroys the electroactivity of the first step and results in an overall four-electron, irreversible reduction. Voltammetric peak shapes are controlled by the competition between reaction pathways for the hydrazo form. In the present case, in buffered solution, the second reaction step is pseudo-first-order.

(12) Bishop, E., Ed. *Indicators*; Pergamon Press: New York, 1972; p 77.

(13) Gurr, E. *Synthetic Dyes in Biology, Medicine, and Chemistry*; Academic Press: New York, 1971; p 32.

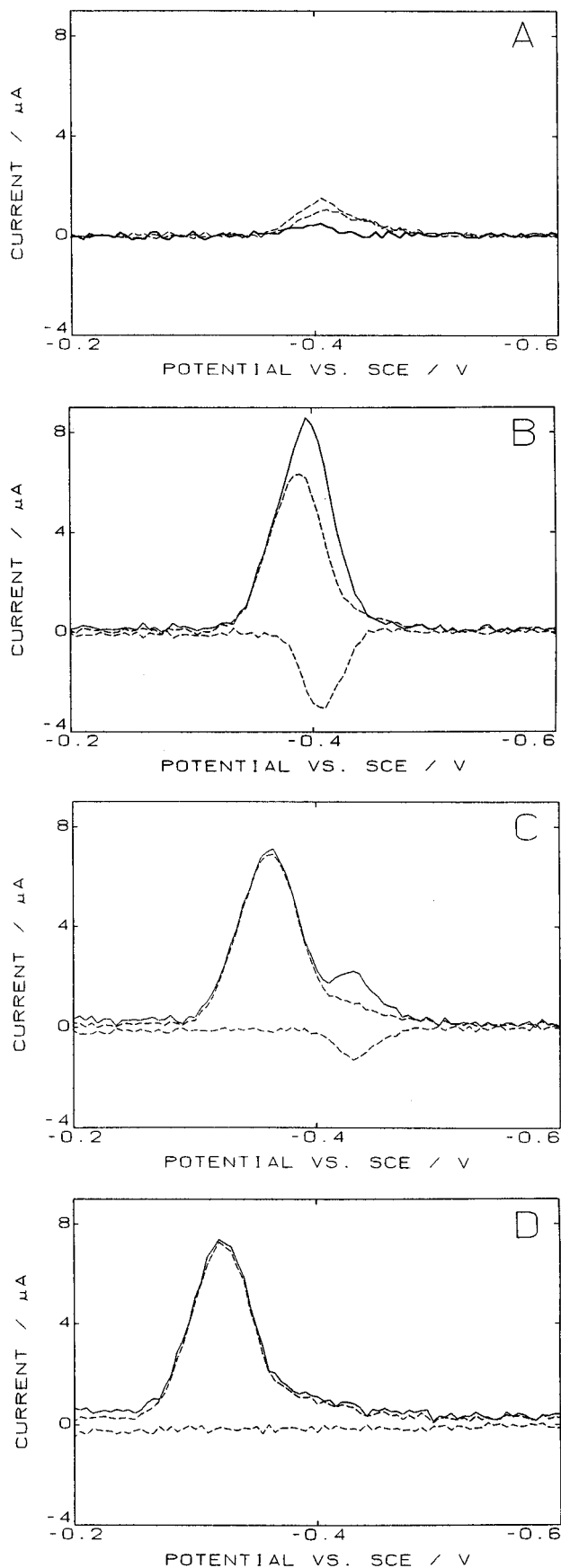


Figure 7. Experimental voltammograms for 10 μM Dimethyl Yellow at pH 6.00. Twenty voltammograms were averaged for each amplitude. Accumulation time, $t_c = 5$ s; $E_c = -0.2$ V vs SCE; $t_p = 5.0$ ms ($f = 100$ Hz); $\Delta E_s = 5$ mV. Upper dashed curves are forward currents. Lower dashed curves are reverse currents. Solid curves are net currents. $E_{sw} =$ (A) 0, (B) 30, (C) 60, and (D) 100 mV.

Table 1. Results of Analysis of Forward and Reverse Currents by the COOL Algorithm^a

E_{sw}^b	$E_1^0{}^c$	α_1^d	$k_1^0{}^e$	α_2^f	$k_2^0{}^g$	a^h	SD ⁱ	R ^j
0	-0.399	0.474	93.6	0.130	10.85	39.9	0.065	0.9823
10	-0.399	0.470	99.5	0.099	11.10	44.2	0.073	0.9952
20	-0.399	0.464	100.8	0.080	11.99	44.0	0.092	0.9969
30	-0.398	0.445	102.4	0.117	11.60	44.0	0.093	0.9980
40	-0.398	0.443	104.4	0.111	12.00	44.3	0.102	0.9979
50	-0.398	0.441	104.1	0.113	11.92	45.0	0.124	0.9970
60	-0.398	0.429	107.0	0.124	11.20	44.5	0.125	0.9967
70	-0.398	0.430	105.7	0.144	9.33	44.5	0.145	0.9956
80	-0.397	0.422	104.5	0.138	8.64	44.3	0.155	0.9950
90	-0.396	0.425	98.3	0.161	6.41	44.5	0.163	0.9947
100	-0.396	0.427	97.8	0.139	6.42	45.1	0.188	0.9930
POOL ^k	-0.397	0.426	102.6	0.110	11.12	44.1	0.137	0.9953

^a Dimethyl Yellow, 10 μM ; $E_c = -0.20$ V; $t_c = 5$ s; $\Delta E_s = 5$ mV; frequency = 100 Hz; 20 replicates ensemble averaged for each amplitude. ^b Square wave amplitude/mV. ^c Standard potential vs SCE/V (first step). ^d Transfer coefficient (first step). ^e Standard rate constant/ s^{-1} (first step). ^f Transfer coefficient (second step). ^g Standard rate constant/ s^{-1} (second step, referenced to E_1^0). ^h Proportionality constant $a/\mu\text{A}$ (eq 40). ⁱ Standard deviation from the model/ μA . ^j Correlation coefficient for i_{obs} vs Ψ . ^k Results for pooled voltammograms, $E_{sw} = 0-100$ mV.

The ability to calculate voltammograms such as Figures 3–6 is required in order to obtain values of parameters from experimental data using the COOL algorithm.⁴ In this method, the observed current, i_{obs} , is modeled as a linear function of the dimensionless current, Ψ . Hence,

$$i_{obs} = a\Psi(\alpha_1, \alpha_2, \kappa_1^0, \kappa_2^0, E_1^0) + b + \epsilon \quad (40)$$

Here, ϵ is random experimental error, b is an arbitrary bias in the experimental data set, and a is the proportionality constant between the observed current and dimensionless current, defined by (cf. eq 30)

$$a = \frac{(n_1 + n_2)FA_e\Gamma^*}{t_p} \quad (41)$$

The amplitude of the response is scaled by this proportionality constant. Peak shapes, however, are controlled by the five nonlinear parameters of Ψ . The COOL algorithm employs a five-dimension search to maximize the correlation coefficient of eq 40. If the model is complete and correct, then the resulting optimal values of parameters are best estimates in the least-squares sense. Since the pulse width, t_p , is defined by the waveform, standard rate constants follow directly from the definitions of the dimensionless standard rate constants (eqs 35 and 36). The value of the proportionality constant, a , is obtained also from COOL. As can be seen from eq 40, this is just the slope of a plot of observed current against dimensionless current, i_{obs} vs Ψ . If the area of the electrode is known, then the value of a yields the total surface concentration of adsorbates, Γ^* .

Table 1 gives values of parameters for the two-step model obtained by COOL analysis over a wide range of square wave amplitudes. The excellent agreement between the model and experiment can be judged from the standard deviation from the model and the correlation coefficient for i_{obs} vs Ψ . Experimental voltammograms were not background subtracted and hence contain a small amount of charging current, which increases with

Table 2. Results of Analysis of Forward and Reverse Currents by the COOL Algorithm^a

f^b	$E_1^0{}^c$	α_1^d	$k_1^0{}^e$	α_2^f	$k_2^0{}^g$	a^h	SD^i	R^j
100	-0.398	0.432	101.8	0.095	11.44	41.6	0.084	0.9982
125	-0.399	0.446	98.2	0.083	11.67	55.1	0.094	0.9988
150	-0.398	0.441	94.8	0.084	10.32	69.3	0.091	0.9993
175	-0.398	0.439	92.0	0.091	9.63	83.6	0.095	0.9995
200	-0.397	0.435	87.6	0.095	8.46	103.6	0.097	0.9996
225	-0.398	0.441	86.1	0.091	8.76	117.5	0.103	0.9996
250	-0.397	0.441	85.4	0.100	8.16	130.5	0.126	0.9995
275	-0.397	0.440	84.6	0.106	7.94	147.4	0.154	0.9993
300	-0.397	0.439	84.1	0.109	7.72	163.5	0.180	0.9991
325	-0.397	0.442	84.0	0.113	7.85	177.1	0.202	0.9990
350	-0.397	0.439	84.3	0.117	7.65	192.0	0.243	0.9986
375	-0.397	0.438	84.4	0.114	7.62	209.1	0.296	0.9981
400	-0.397	0.432	83.9	0.117	7.40	227.3	0.337	0.9977

^a Dimethyl Yellow, 10 μM ; $E_c = -0.20$ V; $t_c = 5$ s; $\Delta E_s = 5$ mV; $E_{sw} = 30$ mV; 20 replicates ensemble averaged for each frequency. ^b Square wave frequency/Hz. ^c Standard potential vs SCE/V (first step). ^d Transfer coefficient (first step). ^e Standard rate constant/ s^{-1} (first step). ^f Transfer coefficient (second step). ^g Standard rate constant/ s^{-1} (second step, referenced to E_1^0). ^h Proportionality constant $a/\mu\text{A}$ (eq 40). ⁱ Standard deviation from the model/ μA . ^j Correlation coefficient for i_{obs} vs Ψ .

pulse amplitude. This can be seen in Figure 7 as an increasing separation of the forward and reverse current baselines as the square wave amplitude increases. Although the standard deviation from the model increases slightly because of this effect, the correlation coefficient of i_{obs} vs Ψ remains high except for weak signals partially masked by noise, i.e., for $E_{sw} = 0$ mV. The model parameters are largely independent of square wave amplitude and quantitatively describe the wide variety of peak shapes shown in Figure 7. The proportionality constant, a (cf. eq 40), is also constant in spite of the drastic changes occurring in peak size, shape, and position. Pooling voltammograms yields a common a of 44.1 μA , which corresponds to a surface coverage of 17.3 pmol cm^{-2} under these conditions of concentration and accumulation time. Optimal parameters for the pooled set of voltammograms are as follow: $E_1^0 = -0.397 \pm 0.001$ V vs SCE; $\alpha_1 = 0.43 \pm 0.02$; $k_1^0 = 103 \pm 8$ s^{-1} ; $\alpha_2 = 0.11 \pm 0.04$; and k_2^0 (referenced to E_1^0) = 11.1 ± 1.7 s^{-1} . Uncertainties are the 95% confidence intervals associated with each parameter.⁴

A direct comparison between the experimental voltammograms of Figure 7 and the currents predicted by the model parameters is given in Figure 8. The relative position, height, and detailed shapes of the voltammograms are predicted remarkably well by the two-step model.

The robustness of the two-step model is further demonstrated by the constancy of the calculated rate constants over a range of square wave frequencies. Table 2 shows this result over the range 100–400 Hz. Unlike the previous case, where the square wave amplitude was varied, the proportionality constant, a , changes linearly with square wave frequency, as predicted by eq 41.

For planar electrodes, a is also related to the bulk diffusion coefficient of the species, D , by

$$a = \left(\frac{2(n_1 + n_2)FA_e D^{1/2} C^*}{\pi^{1/2} t_p} \right) t_c^{1/2} \quad (42)$$

where C^* is the bulk concentration of the adsorbate. This

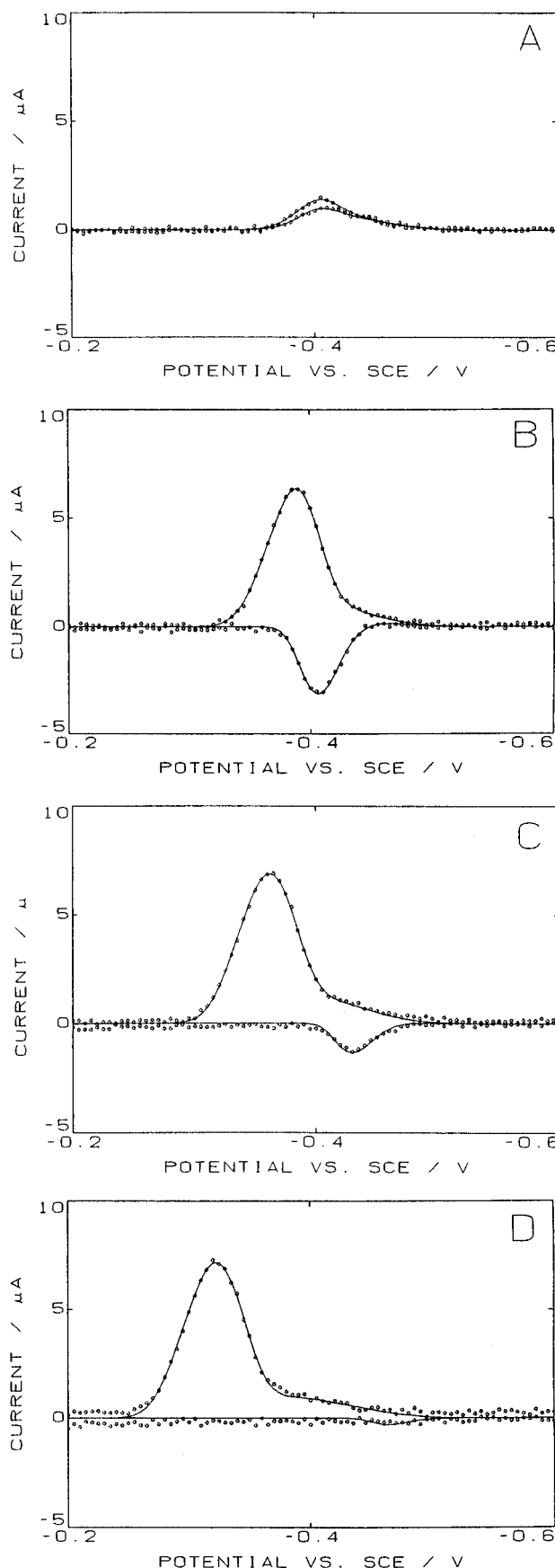


Figure 8. Two-step model curves compared with experimental voltammograms. Conditions are the same as for Figure 7. Model parameters are given in Table 1. Forward and reverse experimental currents (O); calculated forward and reverse model currents (—). $E_{sw} =$ (A) 0, (B) 30, (C) 60, and (D) 100 mV.

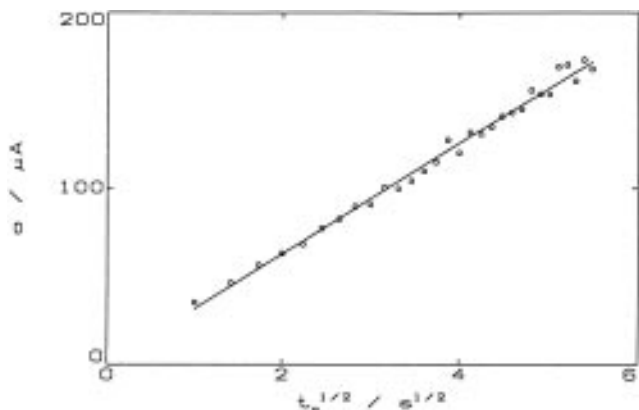


Figure 9. a vs $t_c^{1/2}$ from experimental voltammograms of $10 \mu\text{M}$ Dimethyl Yellow at pH 6.00. Three voltammograms were averaged for each accumulation time. $t_c = 1\text{--}30$ s; $E_c = -0.2$ V vs SCE; $t_p = 5.0$ ms ($f = 100$ Hz); $\Delta E_s = 5$ mV; $E_{sw} = 30$ mV.

relationship is obtained from the definition of a and the integrated form of the Cottrell equation. For our experimental conditions, the contribution of spherical diffusion is, at most, only a few percent. A plot of a vs $t_c^{1/2}$ should be linear with a slope proportional to $D^{1/2}$. This is observed experimentally, as can be seen in Figure 9. The slope a vs $t_c^{1/2}$ provides an estimate of the value of D that is otherwise difficult to obtain. Normal pulse voltammograms of dilute solutions of the dye exhibit large maxima and strongly sloping plateaus. The bulk concentration of the dye cannot be greatly increased because of poor solubility. The use of mixed solvents (typically alcohol–water mixtures) introduces additional adsorbates and changes the solvent matrix and hence the value of the diffusion coefficient. The diffusion coefficient value of Dimethyl Yellow calculated from the slope of Figure 9 is $1.2 \times 10^{-6} \text{ cm}^2 \text{ s}^{-1}$. For very long accumulation times ($t_c > 250$ s), linearity is lost, and the mercury surface saturates with an apparent maximal coverage of 186 pmol cm^{-2} .

Note that peak current depends on the value of Ψ , which is a function of both experimental and kinetic parameters. The slope, a , provides a much more robust measure of amplitude, and hence of surface concentration. By means of relations such as eq 42, the slope also yields concentration in solution. The advantage of such mathematical treatments for the enhancement of the performance of voltammetric sensors has already been demonstrated for several systems not involving adsorption.¹⁴ We have used this approach with the two-step model to examine, in less detail, the electrochemical reaction of a large number of adsorbed

azo dyes.¹⁵ The model has proven applicable and useful in these cases and should apply also to many classes of organic compounds in buffered aqueous solution.

CONCLUSIONS

A comprehensive description of the voltammetric behavior of a redox-modified surface undergoing redox cycling coupled with irreversible surface reaction has been formulated from first-order chemical kinetics. This model, used with square wave voltammetry and nonlinear least-squares analysis (COOL), provides the means to characterize quickly the electrochemical properties of interfacial systems such as that employed here, Dimethyl Yellow adsorbed on mercury. Thermodynamic, kinetic, and analytical information is obtained from analysis of the square wave voltammetric response.

The first-order model yields a closed-form expression for current, which makes the computation very fast. Computational speed makes it practical to examine the morphology of the response for a range of parameters, such as pulse amplitude, and renders kinetic and analytical information from experimental currents in a second. The first-order model surrenders little in generality, in that pseudo-first-order conditions can be found for broad categories of reactions, in particular for redox enzymes adsorbed at modified electrodes in buffered aqueous solution.

The square wave waveform possesses the advantage that time (frequency) and potential (square wave amplitude) can be varied independently to produce the desired sensitivity and resolution for the investigation complex surface reactions. Kinetic response depends only weakly on time, but very strongly on potential. The combination of square wave voltammetry and COOL makes practical the elucidation of mechanism from the dependence of the response on square wave amplitude.

From the analytical point of view, the response can be adjusted to produce one well-shaped peak at a favorable potential. From the kinetic point of view, the response can be tuned to emphasize features especially sensitive to rate processes, and this yields efficiently kinetic parameters of acceptable quality.

ACKNOWLEDGMENT

The authors thank Bioanalytical Systems Inc. for the donation of the controlled growth mercury electrode and Gang Xu for important preliminary work. This work was supported in part by the National Science Foundation under Grant No. CHE9208987.

Received for review July 2, 1996. Accepted November 8, 1996.[⊗]

AC960647V

(14) Chin, K. Y.; Prasad, S.; O'Dea, J. J.; Osteryoung, J. *Anal. Chim. Acta* **1992**, *264*, 197.

(15) Xu, G.; O'Dea, J. J.; Osteryoung, J. G. *Dyes Pigments* **1996**, *30*, 201.

[⊗] Abstract published in *Advance ACS Abstracts*, January 1, 1997.